CrossMark

Experimental analysis of the dynamical response of energy harvesting devices based on bistable laminated plates

A. Syta · C. R. Bowen · H. A. Kim · A. Rysak · G. Litak

Abstract The use of bistable laminates is a potential approach to realize broadband piezoelectric based energy harvesting systems. In this paper the dynamic response of a piezoelectric material attached to a bistable laminate plate is examined based on the experimental generated voltage time series. The system was subjected to harmonic excitations and exhibited single-well and snap-through vibrations of both periodic and chaotic character. To identify the dynamics of the system response we examined the frequency spectrum, bifurcation diagrams, phase portraits, and the 0–1 test.

1 Introduction

Recently, various energy harvesting devices have been developed in an attempt to convert ambient vibrations to electrical energy [1, 2]. This interest has stemmed from the need to develop autonomous low-powered electronic systems such as wireless sensor networks and safety monitoring systems. For vibration harvesting the use of piezoelectric materials is a potential route for generating the necessary power levels, typically in the μW to mW range. The advantages of these materials are their higher strain energy densities compared to electrostatic and electromagnetic systems and their ease of integration with mechanically vibrating structures [3].

In many cases, such as those on railway carriages [4] or other forms of transport [5, 6], the ambient vibrations can exhibit multiple time-dependent frequencies, may change with time and can include components at relatively low frequencies. It has been reported that introducing nonlinear effects can lead to an improvement of the frequency bandwidth of the vibration energy harvester [7].

As a result, a variety of approaches for incorporating non-linearity in the stiffness of energy harvesters have been considered, most notably by designing bistable harvesters with two distinct energy wells [8–13] using repulsive or attractive magnetic interactions between a cantilever and an external magnet, axial loading of canilevers and the use of post-buckled beams.

An alternative method of developing bistability was reported by Arrieta et al. [14–18] where a piezoelectric element was attached to an asymmetric bistable laminate plate made from a carbon fibre reinforced polymer (CFRP) laminate with a $[0/90]_T$ layup. Due to the difference in the coefficient of thermal expansion between the carbon fibre and epoxy matrix the thermal residual stress developed on cooling of the laminate

A. Syta · A. Rysak · G. Litak (✉)
Faculty of Mechanical Engineering, Lublin University of Technology, Nadbystrzycka 36, 20-807 Lublin, Poland
e-mail: g.litak@pollub.pl

C. R. Bowen · H. A. Kim
Department of Mechanical Engineering, University of Bath, Bath BA2 7AY, UK

from an elevated cure temperature leads to it exhibiting two distinct stable states. When subjected to large amplitude oscillations the laminate undergoes snap-through between the two stable states. For energy harvesting [19] when a piezoelectric material is attached to the bistable laminate surface it can generate power by repeated straining as it experiences deformation as a result of mechanical vibrations. Experimentally, such harvesting devices have been shown to exhibit high levels of power extraction over a wide range of frequencies when harmonically excited from a central mounting [20], with the scope for improved power generation through changes in the geometry. The potential advantages of using the intrinsic thermal stress in the laminate to induce bistability, compared to using magnetic configurations [19, 21] is that (1) the laminate can be designed to occupy a smaller space and there are no stray magnetic fields, (2) the laminate can be readily combined with piezoelectric materials and (3) there is potential to tailor the laminate lay-up, laminate elastic properties and geometry to provide additional control over the harvester response to the vibrations that are being harvested.

In the present work we employ an electro-mechanical system to generate mechanical vibrations leading to snap-through of the laminate between its two stable states. Such a system has the potential of have a broadband frequency response in terms of its voltage output. At this stage it is of interest to note that a monostable system is characterized by a single potential well while a bistable by a double potential well. In contrast to the simplest mono-stable linear system, which shows narrow frequency resonance, bistable structures are inherently nonlinear and are characterized by an inclined (nonsymmetric) resonance curve covering the wider region of frequencies. Another effect caused by strongly nonlinear bistable system can be the appearance of multiple solutions. In such a case, the solutions can be grouped into the hopping cases with large amplitudes and those sitting in the single potential well with small amplitude of oscillations. The advantage of a bistable resonator is visible for lower frequencies. In our system of a bistable plate, hopping between potential wells is realized by a snap-through phenomenon. Due to the linear coupling between displacement and voltage in a piezoelectric patch, a larger vibration of amplitude response for given excitation frequency implies larger power output.

The motivation of this work is to develop methods to identify the bistable mechanical resonator response to vibrations; these include single well oscillations, continuous snap-through between stable states and the existence of chaotic or periodic snap-through behaviour [20, 22]. An understanding of the nature of the complex dynamic response of such a system could be used to optimise the ambient vibration energy harvesting.

2 Experimental setup

A square $[0/90]_T$ carbon fibre reinforced laminate was considered as the basis for developing a broadband energy harvesting device. The laminate measured 190 mm by 190 mm and was made from M21/T800 CFRP prepreg material. A single piezoelectric Macro Fiber Composite (MFC) layer (M8585-P2, 85 mm × 85 mm) was bonded to the laminate surface. Figure 1a shows the two stable state of the CFRP-MFC combination which is mounted to an electrodynamic shaker (LDS V455) at its centre, see Fig. 1b. Note that in most cases, application of MFC with interdigitated electrode (IDE), where the polarisation direction is along the fibre length, is characterised by a low efficiency for energy harvesting comparing to a mono-fiber piezo-ceramic element (PZT) [23–25]. In this case the M8585-P2 device is polarised through thickness by continuous upper and lower electrodes. Compared to an IDE based device such a configuration has (1) a more uniform electric field distribution (2) a high device capacitance, leading to low peak voltages as a result of the piezoelectric charge and (3) a low electrical impedance due to the high device capacitance. The MFC has also an advantage in better flexibility. This property is crucial in our system as the axis of bending is changing due to bistability of a plate.

3 Experimental results

Under kinematic excitation the laminate plate can show a variety of responses reflected in the measurement of the open-circuit voltage. In Fig. 2 we show the results for a sampling frequency of 1000 Hz.

The voltage-time response as a result of vibration testing with a 10g peak acceleration at frequencies

(a)

(b)

Fig. 1 a The laminate used for these tests measures 190 mm × 190 mm × 0.5 mm, has a [0/90]$_T$ layup and has a single piezoelectric layer Micro-Fibre-Composite (MFC) attached to the top surface of dimensions 85 mm × 85 mm × 0.3 mm, and **b** experimental setup showing mechanical shaker attachment

Fig. 2 Voltage time series of experimental results corresponding for increasing frequencies $f = 30, 35, 40, 45, 50, 51, 55, 57, 60, 65, 70, 75, 80$ Hz corresponding to subplots (**a–m**), respectively. Note single well mode cases (**a–d** and **j-m**), and snap-through buckling cases: regular (**f**, **g**), chaotic (**e**, **h**), and transient chaotic-regular (**i**). Stationary and transient chaotic responses are denoted by *red colour* for better clarity. Each excitation had 10g amplitude acceleration. Sampling frequency was 1000 Hz
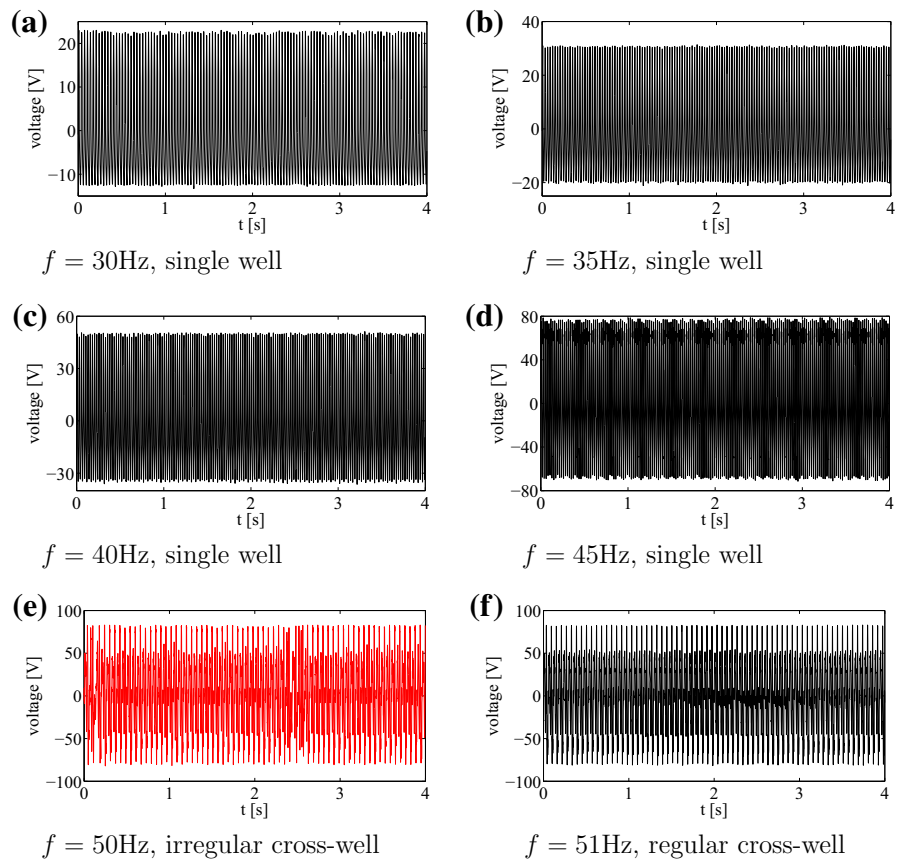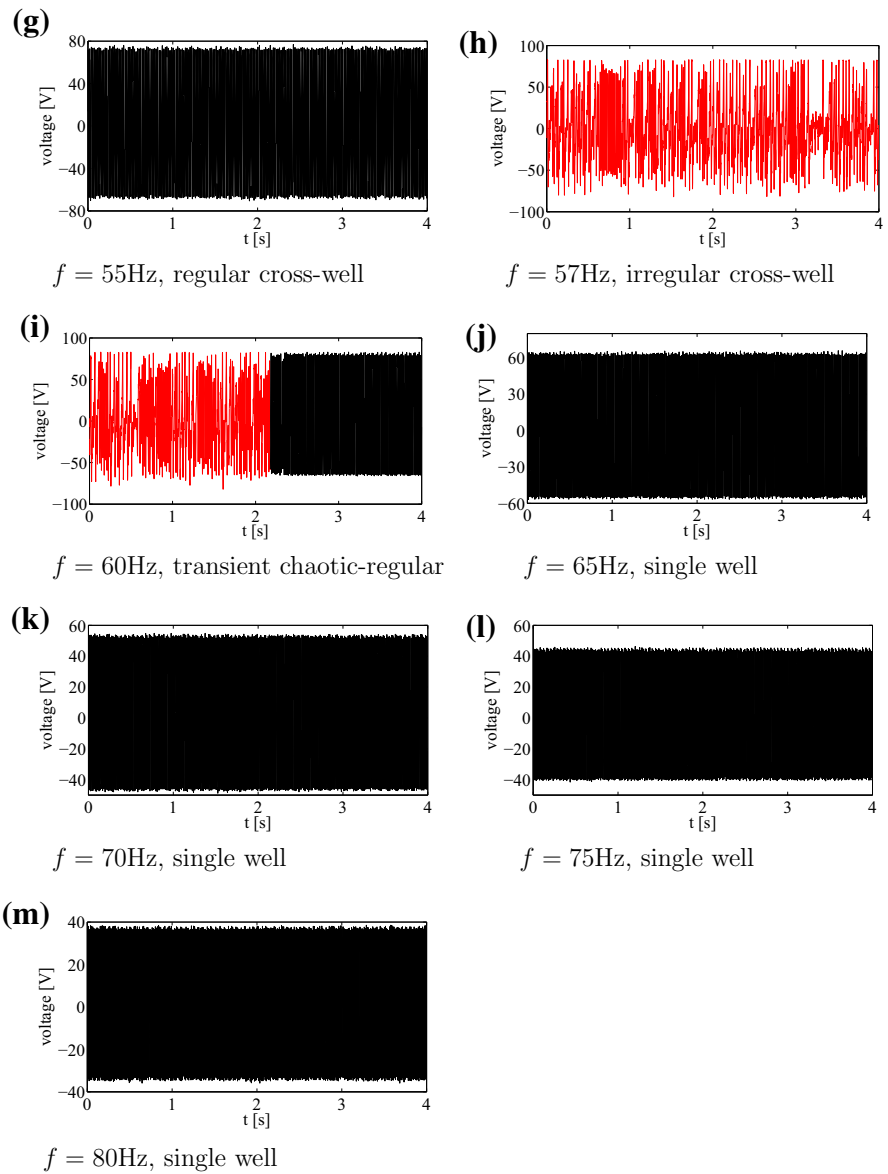

(a) $f = 30$Hz, single well

(b) $f = 35$Hz, single well

(c) $f = 40$Hz, single well

(d) $f = 45$Hz, single well

(e) $f = 50$Hz, irregular cross-well

(f) $f = 51$Hz, regular cross-well

Fig. 2 continued

(g) $f = 55$Hz, regular cross-well

(h) $f = 57$Hz, irregular cross-well

(i) $f = 60$Hz, transient chaotic-regular

(j) $f = 65$Hz, single well

(k) $f = 70$Hz, single well

(l) $f = 75$Hz, single well

(m) $f = 80$Hz, single well

ranging from of 30–80 Hz are summarised in Fig. 2. Interestingly, the voltage-time response exibits both periodic and non-periodic (chaotic) behaviour. In essence the results can be classified as

(1) single well oscillations with no snap-through at small amplitude oscillations, as seen in Fig. 2a–d and j–m,

(2) cross-well oscillations with snap-through at regular intervals (but not every cycle, Fig. 2g),

(3) cross-well oscillations with snap-through at irregular intervals chaotic Fig. 2e, h,

(4) continuous snap-through at every cycle, Fig. 2f.

For better clarity the stationary chaos and transient chaotic responses are denoted by red colour. Figure 2i presents an interesting case where there is transient chaotic-regular behaviour. Schematic images of the possible mode shapes during single well and snap-through are shown in Fig. 3. Figure 4a–m shows the corresponding Fourier transforms of the examined measured voltage output. One can observe that the excitation frequency is accompanied by the higher

harmonics in all the figures. In addition, in Fig. 4e, h, i there is smearing of the discrete frequency response into bands as expected for chaotic cases. Note that the frequency spectra represent a qualitative criterion of the system response. In the discussion below, the nature of the dynamic behavior of the responses will be explained using established tools.

Interestingly, the more complex response cases are close to the resonance region. This has been summarised in Fig. 5a which is a bifurcation map created from the local maxima collected from cycles in the corresponding votage time series (Fig. 2). One can distinguish the regular and chaotic responses as singluar points and point bands, respectively. Note the case $f = 51$ Hz is not a

Fig. 3 Vibration modes of a bistable square plate **a** single well: small amplitude vibrations around one of the equilibrium states; **b** snap-through: large amplitude vibrations
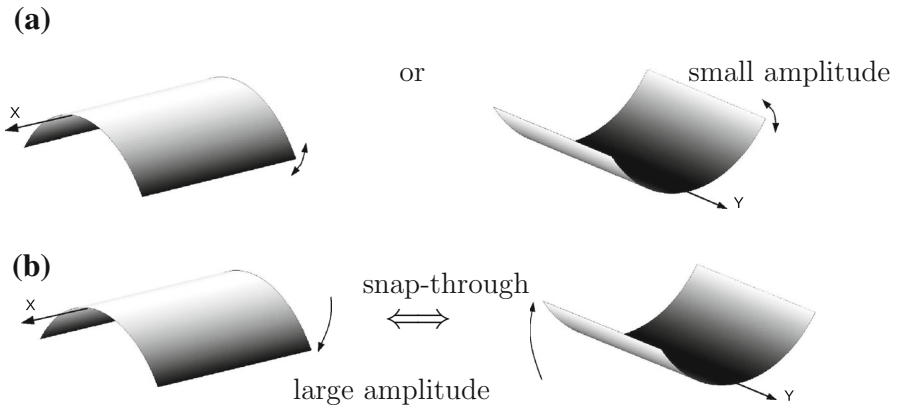
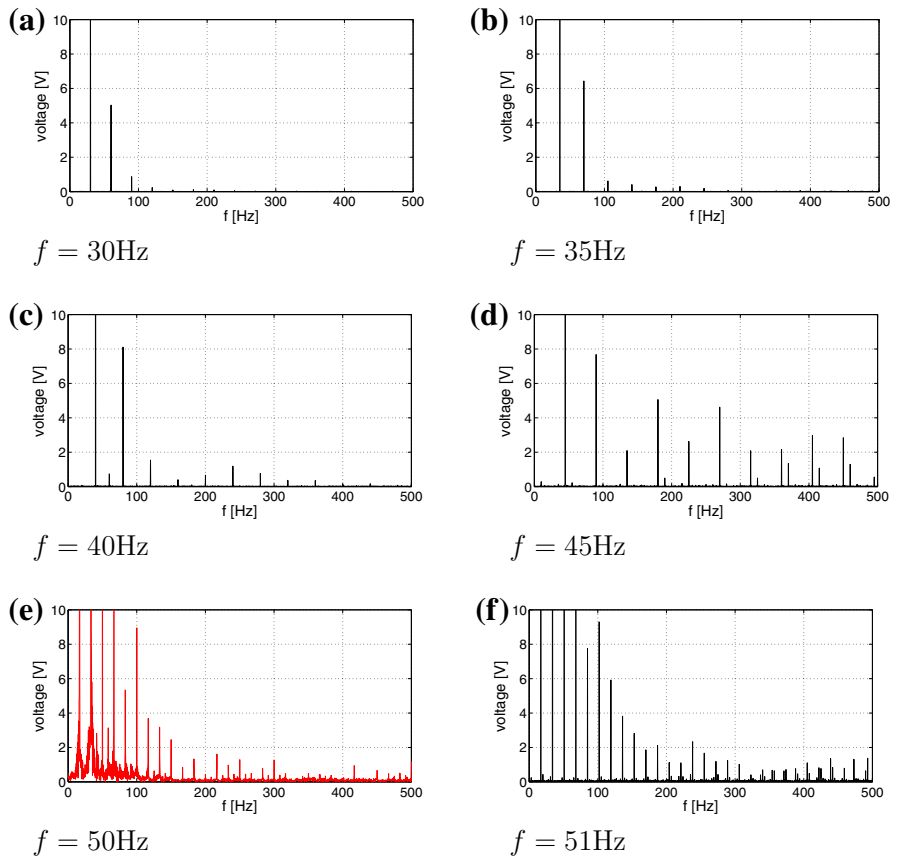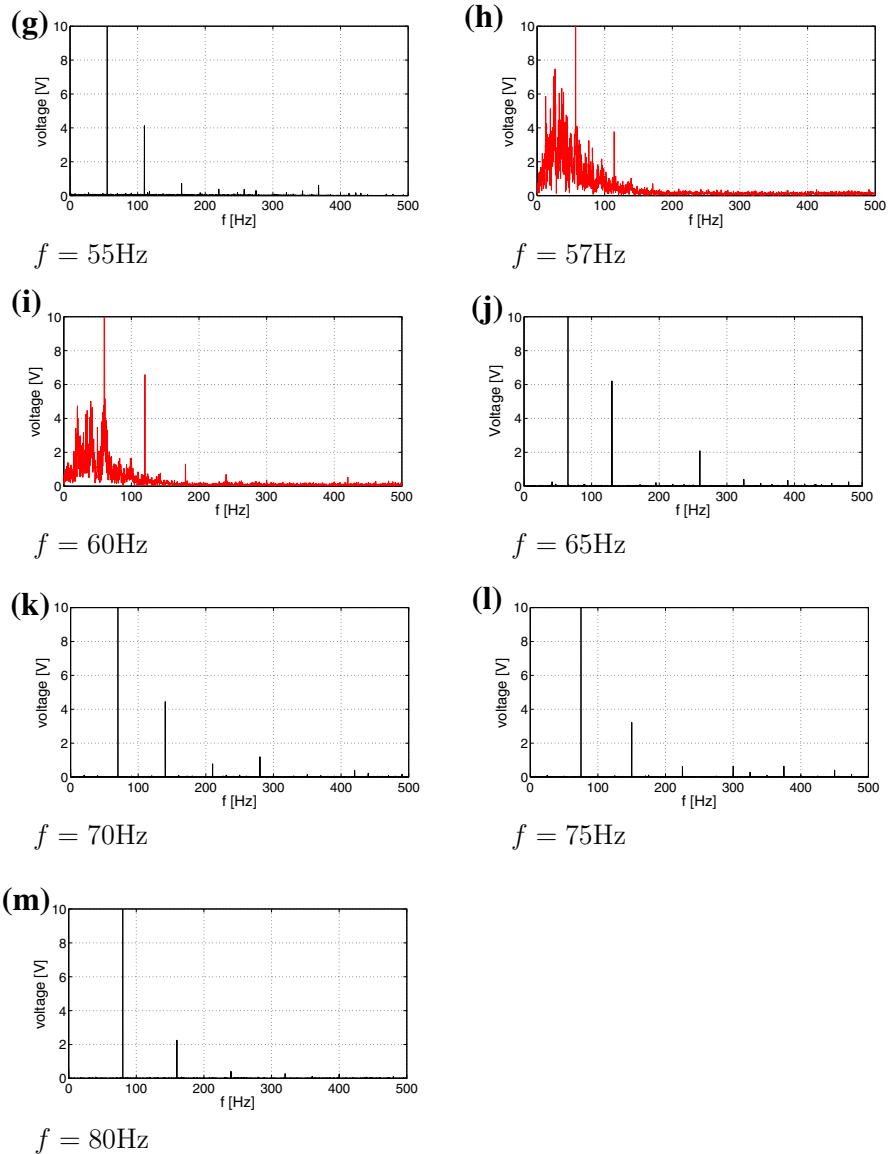**Fig. 4** Frequency spectra (**a**–**m**) corresponding to voltage time series Fig. 2a–m, respectively

Fig. 4 continued

(g)

$f = 55\,\mathrm{Hz}$

(h)

$f = 57\,\mathrm{Hz}$

(i)

$f = 60\,\mathrm{Hz}$

(j)

$f = 65\,\mathrm{Hz}$

(k)

$f = 70\,\mathrm{Hz}$

(l)

$f = 75\,\mathrm{Hz}$

(m)

$f = 80\,\mathrm{Hz}$

clear case and has been clasified as a multifrequency regular case because of the discrete Fourier spectrum (see Fig. 4f). The associated resonance curve is estimated via the voltage output variance $\mathrm{var}(u) = \sigma_u^2$ which is plotted versus frequency f (Fig. 5b). Note that the large voltage response is acompanied by cross-well oscillations of regular and chaotic nature. Interestingly, chaotic oscillations are characterised by a smaller voltage output (see red points in Fig. 5b).

In the next sections, we propose to use the 0–1 test for more accurate chaos identification.

4 The '0–1 test'

The '0–1 test', invented by Gottwald and Melbourne [26, 27], can be applied for any system of a finite dimension to identify the chaotic dynamics but it is based on the statistical properties of a single coordinate only. Thus it is suitable to quantify the response where only one parameter was measured in time. As it is related to the universal properties of the dynamical system such as spectral measures, it can distinguish a chaotic system from a regular one.

(a)

(b)
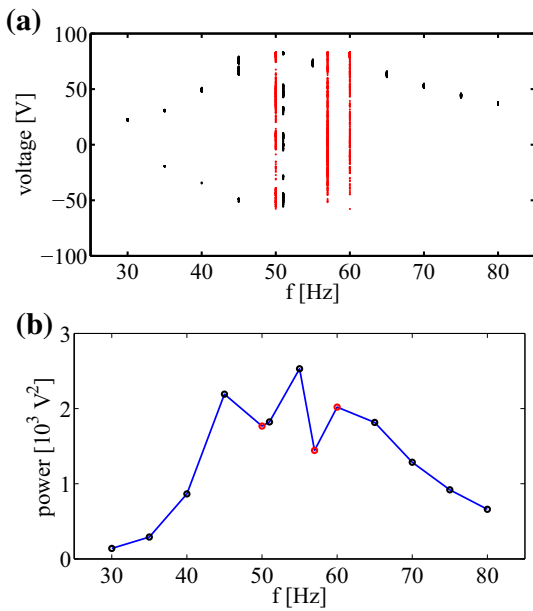
Fig. 5 Bifurcation diagram (**a**)—created on the basis of local maximum points of the corresponding time series (Fig. 2), resonance curve (**b**)—var(u) versus frequency f. Note, the *red points* correspond to chaotic oscillations (see f = 50, 57, and 60 Hz)

A particular advantage of the 0–1 test over the frequency spectrum is that it provides information regarding the dynamics in a single parameter value, similar to the Lyapunov exponent. However, the Lyapunov exponent can be difficult to estimate in any non-smooth simulated or measured data [31]. The present system (Fig. 1) used an asymmetric bistable laminate plate as an example showing non-linear elastic properties. Therefore the 0–1 test can provide the suitable algorithm to identify the chaotic solution [32–35].

Starting from the voltage output $u(i)$, for sampling points $i = 1, \ldots, N_t$, (where $N_t = 4000$) we define new coordinates $p(n)$ and $q(n)$ as

$$p(n) = \sum_{j=0}^{n} \frac{(u(j) - \overline{u})}{\sigma_u} \cos(jc),$$

$$q(n) = \sum_{j=0}^{n} \frac{(u(j) - \overline{u})}{\sigma_u} \sin(jc), \tag{1}$$

where $\overline{u}$ denotes the average value of u while σ_u its standard deviation, c is a constant $\in [0, \pi]$. Note that $q(n)$ is a complementary coordinate in the two dimensional space. Furthermore, starting from bounded coordinate $u(i)$ we build a new series of $p(n)$ which

can be either bounded or unbounded depending on dynamics of the examined process.

Continuing the calculation procedure, the total mean square displacement is defined as

$$M_c(n) = \lim_{N \to \infty} \frac{1}{N} \sum_{j=1}^{N} [(p(j + n) - p(j))^2 + (q(j + n) - q(j))^2], \tag{2}$$

The asymptotic growth of $M_c(n)$ can be easily characterized by the corresponding ratio $K_c'(n)$

$$K_c'(n) = \frac{\ln(M(n))}{\ln n}. \tag{3}$$

In the limit of a very long time $n \to \infty$ (in practice $n = n_{max} = 400$ while $N = 3600$) we obtain the corresponding values of K_c for a chosen c value. Note, our choice of n_{max} and N limits (in Eqs. 4 and 5) is consistent with that proposed by Gottwald and Melbourne [28–30] $N, n_{max} \to \infty$ but simultaneously n_{max} should be about $N/10$.

It is important to note that the parameter c acts like a frequency in a spectral calculation. If c is badly chosen, it could resonate with the excitation frequency or its ultra- or sub-harmonics. In the 0–1 test regular motion would yield a ballistic behaviour in the (p, q)-plane [28] and the corresponding $M_c(n)$ results in an asymptotic growth rate even for a regular system. The disadvantage of the test, its strong dependence on the chosen parameter c, can be overcome by a proposed modification. Gottwald and Melbourne [28, 33, 34] suggest to take randomly chosen values of c and compute the median of the corresponding K_c-values.
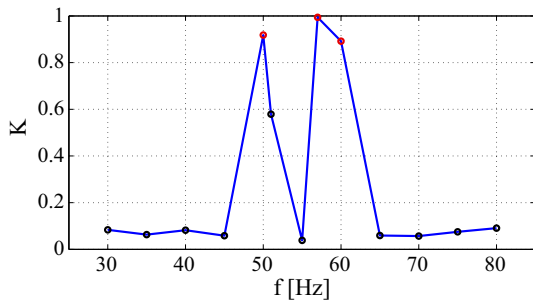
Consequently, the new covariance formulation

$$K_c = \frac{\text{cov}(\mathbf{X}, \mathbf{M}_c)}{\sqrt{\text{var}(\mathbf{X})\text{var}(\mathbf{M}_c)}}, \tag{4}$$

where vectors $\mathbf{X} = [1, 2, \ldots, n_{max}]$, and $\mathbf{M}_c = [M_c(1), M_c(2), \ldots, M_c(n_{max})]$.

In the above, the covariance $\text{cov}(\mathbf{x}, \mathbf{y})$ and variance $\text{var}(\mathbf{x})$, for arbitrary vectors $\mathbf{x}$ and $\mathbf{y}$ of n_{max} elements, and the corresponding averages $\overline{x}$ and $\overline{y}$ respectively, are defined

$$\text{cov}(\mathbf{x}, \mathbf{y}) = \frac{1}{n_{max}} \sum_{n=1}^{n_{max}} (x(n) - \overline{x})(y(n) - \overline{y}),$$

$$\text{var}(\mathbf{x}) = \text{cov}(\mathbf{x}, \mathbf{x}). \tag{5}$$

Fig. 6 Control parameter of the 0–1 test, K (c). $K \to 0$ indicates a regular solution while $K \to 1$ signals chaos. Note, the *red points* correspond to chaotic oscillations (see $f = 50$, 57, and 60 Hz)

Finally, the median is taken of K_c-values (Eq. 6) corresponding to 100 random values of $c \in (0, \pi)$. Such an average K-value can now be estimated for various excitation frequency f. The control parameter K signals the appearance of regular and chaotic solution for K close to 0 and one, respectively.

5 Regular and chaotic oscillations by the '0–1 test'

The results of the parameter K are presented in Fig. 6. We show that for chaotic regions $K \geq 0.9$ while for regular regions K is closer to 0 ($K \leq 0.1$). The case of

Fig. 7 Phase portraits du/dt versus u obtained by numerical differentiation for chosen voltage time series at frequencies **a** $f = 50$ Hz ($K = 0.918$), **b** 51 Hz ($K = 0.579$), **c** 57 Hz ($K = 0.994$), **d** 65 Hz ($K = 0.059$); and finally the transient chaos versus regular cases (see Figs. 2, 6) $f = 60$ Hz ($K = 0.892$) plotted in (**e**) and (**f**), respectively
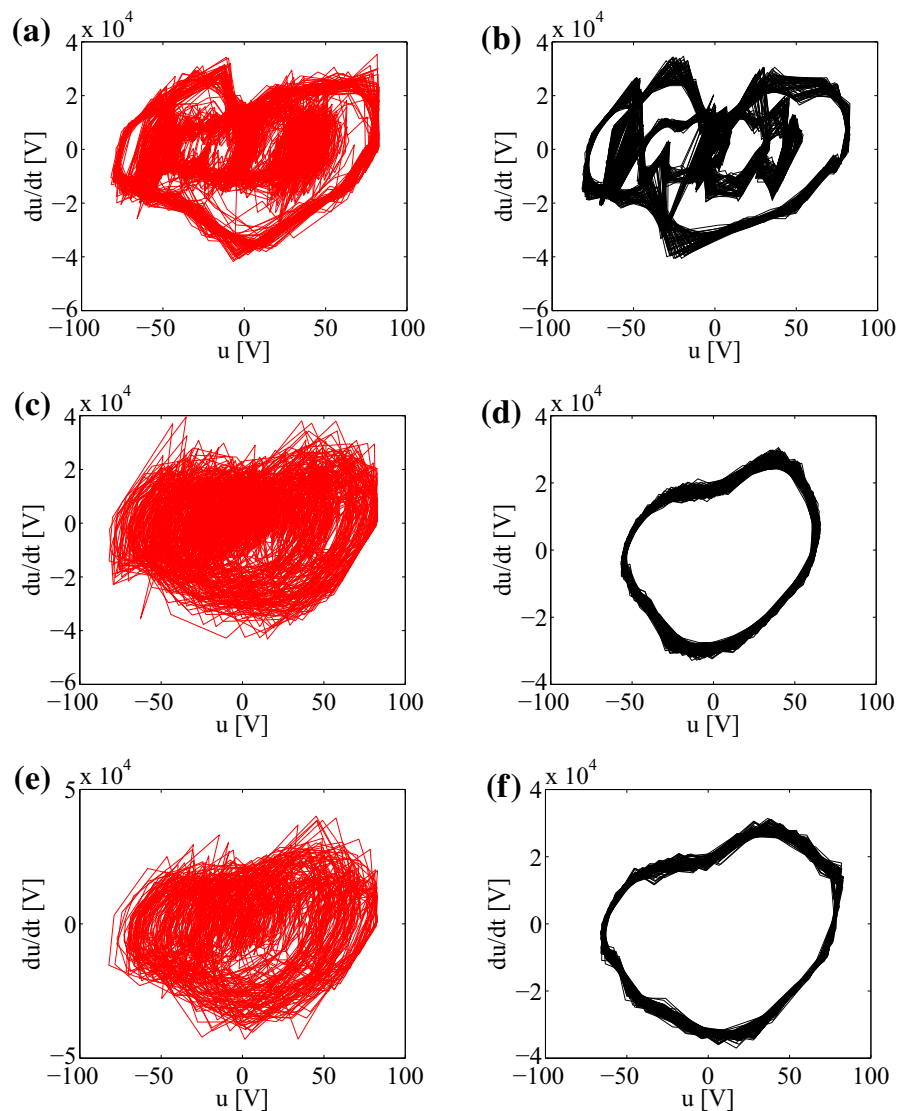
Fig. 8 Phase plane in (p, q)-coordinates for $f = 55$ Hz (regular—**a**) and $f = 57$ Hz (chaotic—**b**) estimated for $c = 1$. The corresponding values of K_c were estimated as $K_c = 0.066$ and $K_c = 0.988$ for cases **a** and **b**, respectively
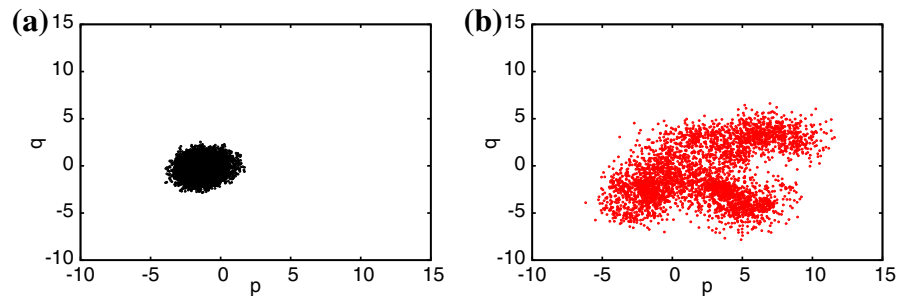
intermediate value (see $K = 0.58$ for $f = 51$ Hz in Fig. 6) signals the vicinity to bifurcation points (see $f = 51$ Hz in the bifurcation diagram Fig. 5a) or a very long transient. In such cases a longer time series can outweigh the classification assignment to a regular response.

For selected chaotic and neighbour frequency cases we now plot the corresponding phase portraits (Fig. 7). It is possible to differentiate regular responses as the close orbits patterns in contrast to strange chaotic attractors. Interestingly, the transient case shows the clear difference between the initial (transient chaotic) and final (regular) behaviour (Fig. 7e, f, respectively). For better clarity we also show examples of the phase plane in the new (p, q) coordinates (Eq. 1). Figure 8a, b shows the growth of the displacement in regular (Figs. 2f, 4f) and chaotic (Figs. 2f, 4f) solutions suggesting the bounded and unbounded cases. The corresponding values of K_c, $K_c = 0.066$ and $K_c = 0.988$, distinguish unambiguously the regular and chaotic cases.

6 Conclusions

The dynamics of a CFRP bistable laminate combined with a piezoelectric MFC has been examined and the existence of chaotic responses have been successfully identified using the 0–1 test. The results obtained are consistent with quantitative methods such as Fourier frequency spectra and corresponding phase portraits. Note that the present investigations are contaminated by a relatively small measurement noise level which is present in any experimental data. This is visible in the values of $K \approx 0.1$ for regular responses. However, better convergence with $K \to 0$ or 1 was achieved indicating that a distinction between regular and chaotic motion could be achieved if a longer time

series was applied. It is also noted that due to the elastic non-linear properties of the examined system a relevant quantitative characterisation (via Lyapunov exponents) of responses is difficult. A further study may involve more sophisticated time-series approaches with a suitable dimensional space embedding [36].

Note that the above identification could be useful for optimising the energy harvester response to a specific vibration input. By focusing on the resonance region (by comparing Figs. 5a, b, 6) it is possible to observe a less complex motion (smaller K) leading to the higher variance of the voltage output [higher var(u)]. For example local minima in Fig. 5b are correlated with peaks in Fig. 6 for the same frequencies $f = 45$ and 55 Hz. Further studies and needed to draw a more general conclusion on the relationship between the power output and K.

References

1. Sodano HA, Inman DJ, Park G (2004) A review of power harvesting from vibration using piezoelectric materials. Shock Vib Dig 36:197–205

2. Bowen CR, Kim HA, Weaver PM, Dunn S (2014) Piezo-electric and ferroelectric materials and structures for energy harvesting applications. Energy Environ Sci 7:25–44

3. Priya S (2007) Advances in energy harvesting using low profile piezoelectric transducers. J Electroceram 19:167–184

4. Ju SH, Lin HT, Huang JY (2009) Dominant frequencies of train-induced vibrations. J Sound Vib 319:247–259

5. Zhu Q, Guan M, He Y (2012) Vibration energy harvesting in automobiles to power wireless sensors. In: International conference on information and automation conference proceedings, Shenyang, China, 6–8 June 2012. IEEE, China, pp 349–354

6. Wood OJ, Featherston CA, Kennedy D, Eaton M, Pullin R (2012) Optimised vibration energy harvesting for aerospace applications. Key Eng Mater 518:246–260

7. Erturk A, Hoffmann J, Inman DJ (2009) A piezomagnetoelastic structure for broadband vibration energy harvesting. Appl Phys Lett 94:254102

8. Daqaq MF, Masana R (2014) On the role of nonlinearities in vibratory energy harvesting: a critical review and discussion. Appl Mech Rev 66:040801

9. Harne RL, Wang KW (2013) A review of the recent research on vibration energy harvesting via bistable systems. Smart Mater Struct 22:023001

10. Pellegrini SP, Tolou N, Schenk M, Herder JL (2013) Bistable vibration energy harvesters: a review. J Intell Mater Syst Struct 24:1303–1312

11. Stanton CS, McGehee CC, Mann BP (2010) Nonlinear dynamics for broadband energy harvesting: investigation of a bistable piezoelectric inertial generator. Phys D 239:640–653

12. Erturk A, Inman DJ (2011) Broadband piezoelectric power generation on high-energy orbits of the bistable Duffing oscillator with electromechanical coupling. J Sound Vib 330:2339–2353

13. Harne RL, Thota M, Wang KW (2013) Concise and high-fidelity predictive criteria for maximizing performance and robustness of bistable energy harvesters. Appl Phys Lett 102:053903

14. Arrieta AF, Hagedorn P, Erturk A, Inman DJ (2010) A piezoelectric bistable plate for nonlinear broadband energy harvesting. Appl Phys Lett 97:104102

15. Arrieta AF, Hagedorn P (2010) Electromechanical modeling and experimental of a bistable plate for nonlinear energy harvesting. In: Proceedings of the ASME 2010 conference on smart materials, adaptive structures and intelligent systems SMASIS2010

16. Arrieta AF, Delpero T, Bergamini A, Ermanni P (2013) Broadband vibration energy harvesting based on cantilevered piezoelectric bi-stable composites. Appl Phys Lett 102:173904

17. Arrieta AF, Delpero T, Bergamini A, Ermanni P (2013) A cantilevered piezoelectric bi-stable composite concept for broadband energy harvesting. In: Proceedings of SPIE, active and passive smart structures and integrated systems, vol 8688, p 86880G-1

18. Arrieta AF, Ermanni P, Erturk A, Inman DJ (2004) On the snap-through dynamic characteristics for broadband energy harvesting with bi-stable composites. In: Proceedings of SPIE, vol 9057, p 90570Z–1

19. Betts DN, Kim HA, Bowen CR, Inman DJ (2012) Optimal configurations of bistable piezo-composites for energy harvesting. Appl Phys Lett 100:114104

20. Betts DN, Guyer RA, Le Bas P-Y, Bowen CR, Inman DJ, Kim HA (2014) Modelling the dynamic response of bistable composite plates for piezoelectric energy harvesting. In: Proceedings of "AIAA SciTech Conference", Maryland, USA

21. Betts DN, Bowen CR, Kim HA, Gathercole N, Clarke CT, Inman DJ (2013) Nonlinear dynamics of a bistable piezo-electric-composite energy harvester for broadband application. Eur Phys J Spec Top 222:1553–1562

22. Borowiec M, Rysak A, Betts DN, Bowen CR, Kim HA, Litak G (2014) Complex response of a bistable laminated plate: multiscale entropy analysis. Eur Phys J Plus 129:211

23. Bilgen O, Wang Y, Inman DJ (2012) Electromechanical comparison of cantilevered beams with multifunctional piezoceramic devices. Mech Syst Signal Process 27:763–777

24. Sodano HA, Inman DJ (2005) Comparison of piezoelectric energy harvesting devices for recharging batteries. J Intell Mater Syst Struct 16:799–807

25. Sodano HA, Lloyd J, Inman DJ (2006) An experimental comparison between several active composite actuators for power generation. Smart Mater Struct 15:1211–1216

26. Gottwald GA, Melbourne I (2004) A new test for chaos in deterministic systems. Proc R Soc Lond A 460:603–611

27. Gottwald GA, Melbourne I (2005) Testing for chaos in deterministic systems with noise. Phys D 212:100–110

28. Gottwald GA, Melbourne I (2009) On the implementation of the 0–1 test for chaos. SIAM J Appl Dyn Syst 8:129–145

29. Melbourne I, Gottwald GA (2008) Power spectra for deterministic chaotic dynamical systems. Nonlinearity 21:179–189

30. Gottwald GA, Melbourne I (2009) On the validity of the 0–1 test for chaos. Nonlinearity 22:1367–1382

31. Wolf A, Swift JB, Swinney HL, Vastano JA (1985) Determining Lyapunov exponents from a time series. Phys D 16:285–317

32. Litak G, Syta A, Wiercigroch M (2009) Identification of chaos in a cutting process by the 0–1 test. Chaos Solitons Fractals 40:2095–2101

33. Litak G, Schubert S, Radons G (2012) Nonlinear dynamics of a regenerative cutting process. Nonlinear Dyn 69:1255–1262

34. Krese B, Govekar E (2012) Nonlinear analysis of laser droplet generation by means of 0–1 test for chaos. Nonlinear Dyn 67:2101–2109

35. Litak G, Bernardini D, Syta A, Rega G, Rysak A (2013) Analysis of chaotic non-isothermal solutions of thermo-mechanical shape memory oscillators. Eur Phys J Spec Top 222:1637–1647

36. Kantz H, Schreiber T (1977) Non-linear time series analysis. Cambridge University Press, Cambridge